

Systematics in the nanoparticle band gap of ZnS and $Zn_{1-x}M_xS$ ($M = \text{Mn, Fe, Ni}$) for various dopant concentrations

M. Behboudnia and P. Sen*

School of Physical Sciences, Jawaharlal Nehru University, New Delhi-110067, India

(Received 13 September 2000; published 2 January 2001)

We report a detailed study of the formation of semiconductor nanoparticles of the important compound ZnS and its Mn-doped variant $Zn_{(1-x)}Mn_xS$ inside reverse micelle microreactors, by carefully varying the size of the reverse micelles at a fixed Mn concentration with $x = 0.01$. Dynamic light scattering techniques allow us to characterize the microreactor sizes and correlate them with the size of the resultant nanoparticles. Band gap measurements employing UV-visible spectroscopy clearly show that Mn-doped samples have higher band gaps, largely independent of the size of the vessel they were created in. This observation reflects the role of Mn as an inhibitor to the growth of the nanoparticles. This is further strengthened by the observation of inhibition by other elements of the first row transition metals. Substitution with Fe and Ni shows similar trends in band gap (and hence particle size) variation with the reaction chamber size as well as with the dopant concentration x of these elements, while such variations on substitution with Mn are distinct, possibly because the sulfides of Zn and Mn are isostructural.

DOI: 10.1103/PhysRevB.63.035316

PACS number(s): 61.46.+w, 73.22.-f, 61.82.Fk

Interest in the physics of low dimensional materials continues unabated. In the case of semiconductor particles, sizes smaller than the bulk excitonic length become important for observing quantum effects. ZnS is a semiconductor material studied extensively because of its importance. Recently,¹ increase in the photoluminescent efficiency of ZnS as a result of doping with Mn has been reported. Photoexcitation, as claimed by the authors, takes place through the sp manifolds of ZnS but gets transferred to the d manifolds of the transition metal impurity. Emission is believed to follow by the way of a $d-d$ intraion transition (spin forbidden) that becomes partially allowed by perturbation by the host crystal fields.

For a photoexcitation transfer from sp to d , strong hybridization is necessary. In a recent publication, Kennedy *et al.*² addressed this question with an electron paramagnetic resonance measurement of the Mn site. It was seen that near-surface Mn sites have crystal field hyperfine couplings identifiable from the bulk values and these were thought responsible for the enhanced photoluminescence. However, the actual value of the hyperfine splitting parameter g was enhanced for the surface sites, denoting lower covalence between the sp states of ZnS and the d states of Mn. This apparent paradox led the authors to suggest a larger hybridization between the sp states and the excited states of Mn rather than the ground state, to explain the enhanced photoluminescence.

There is greater need to identify in detail the processes operating in nanometer-sized particles. This will lead to better understanding of the roles played by confinement as well as substituted impurities. In this article we present a detailed study of the band gap of ZnS nanoparticles as a function of substituted Mn impurities for a fixed dopant concentration ($x = 0.01$). The reverse micellar technique of preparation allows us to fix the size of the containers where the particles are generated. This determines the nanoparticle size that can ultimately be achieved. Employing dynamic light scattering

to determine the sizes of the reverse micelle containers, we correlate them with the observed band gaps (and hence the sizes of the particles). It is shown that for pure ZnS nanoparticles the band gaps correlate with the reverse micellar sizes, and the dependence is approximated by the relation $E_g = ae^{-W_0/b} + ce^{-W_0/d}$, where a, b, c, d are constants and W_0 is the water-surfactant molar ratio, related to the micellar size. For Mn-substituted ZnS, similar variation in size of the reverse micellar reaction vessels results in particles having considerably larger band gaps and hence smaller dimensions even for the largest vessel size employed. The Mn impurity thus acts as an inhibitor to the growth of the ZnS particles, restricting the maximum sizes to approximately 60 Å. This inference is supported by studying trends in the observed band gaps following incorporation of other first row transition metal dopants, Fe and Ni, whose sulfides are not isostructural with ZnS.

We employ the potential of reverse micelles as microreactors³ for the preparation of nanoparticles. In this technique, water and oil are mixed in the presence of a surfactant. The latter settles at the interface of the water-oil mixture, stabilizing small quantities of water in oil. A uniform size of reverse micelles can be obtained easily with a narrow particle size distribution depending on the water-surfactant molar ratio W_0 . The ZnS particles are prepared by reacting pure AR grade chemicals $Zn(NO_3)_2$ and Na_2S in their reverse micellar forms. The reverse micelles are prepared independently from aqueous solutions of these salts by adding them to a mixture of sodium bis(2-ethylhexyl) sulfosuccinate (AOT), a surfactant, and iso-octane, an oil. The ZnS nanoparticles are formed by rapid mixing of the component reverse micelles; the resultant microemulsions remain clear and transparent. Mn doping is done by dissolving the requisite amounts of $MnSO_4$. Recovery of the nanoparticles is achieved by adding and mixing with hexane containing 0.05M of thiophenol followed by centrifugation. The thiophenol provides capping and prevents coagulation of the ZnS particles.

TABLE I. The measured hydrodynamic diameters D_h and diffusion coefficients D of the reverse micelles, and the estimated diameters D_{est} of the extracted ZnS and $\text{Zn}_{(1-x)}\text{Mn}_x\text{S}$ nanoparticles.

W_0	ZnS			$\text{Zn}_{(1-x)}\text{Mn}_x\text{S}$		
	D_h (nm)	$10^8 D$ (cm ² /s)	D_{est} (nm)	D_h (nm)	$10^8 D$ (cm ² /s)	D_{est} (nm)
2	6	1.512	4	5	1.814	3
4	7	1.295	5	7	1.295	5
6	8	1.134	6	8	1.134	6
8	9	1.008	7	9	1.010	7
10	10	0.907	8	10	0.910	8

Dynamic light scattering studies of the centrifuged reverse micelles containing ZnS particles were carried out employing a 1024-channel correlator, Model 9000-AT, supplied by Brookhaven Instruments, USA. The data were collected employing the CONTIN software provided by the same company. The measurement principles can be found in detail elsewhere.⁴ The spectra were collected at room temperature (300 K), and in all experiments the difference between the measured and calculated baselines was not allowed to go beyond 1%. Excessive baselines arise from dust and other extraneous impurities; such samples were rejected. The correlograms were analyzed through a nonlinear Laplace inversion routine to check for relaxation time distributions. Once the unimodal particle size distributions were confirmed, the particle sizes were determined through the CONTIN software.

UV-visible spectra of the samples in the reverse micelle form were collected employing a Hitachi U-3300 spectrophotometer, Japan, using quartz cuvettes of optical path length 1 cm.

The hydrodynamic diameters of the reverse micelles are determined by a well established light scattering technique.⁵ Here it is assumed that light is essentially scattered by concentration fluctuation of the reverse micelles in the continuous phase. Experimentally, excess scattering of light from an Ar ion laser source, due to the particles in the continuous phase, is recorded. The scattered intensities are recorded at a fixed scattering angle of $\theta=90^\circ$ and are relative. Calibration was made employing standard polystyrene latex spheres with known diameters.

The autocorrelation function of the scattered light is given by

$$g^{(2)}(\tau) = 1 + e^{-2DK^2\tau},$$

where $K=(4\pi n/\lambda)\sin(\theta/2)$ and D is the diffusion coefficient. Assuming the reverse micelles to be hard spheres, the hydrodynamic diameters and diffusion coefficients of the colloidal dispersion of ZnS, in reverse micellar media of 100 mM AOT-isooctane at different W_0 values are measured. These are listed in Table I for ZnS and $\text{Zn}_{1-x}\text{Mn}_x\text{S}$. These data show that with increase in the water content through increase in W_0 the size of the reverse micelles increases. Consequently, the diffusion coefficient decreases. The hydrodynamic diameters in this table contain contributions from the AOT molecules which are at the interface between water and oil as well as the reaction products created inside the micelles. Assuming a spherical shape of the

particles measured and subtracting twice the length of the AOT molecules, about 2.0 nm, from each measured hydrodynamic diameter allows us to predict the size of the intended nanoparticles. This is also shown in Table I.

It is thus evident that the size of the reverse micelles, which act like microreactors, can be modified quite easily. The variation of translational diffusion coefficients D with the volume fraction of the dispersed phase ϕ ,⁶ corresponding to 1% (w/v) of reactants and 100 mM AOT at different W_0 , is important to know the distribution in the micellar sizes. The concentration dependence of $D(\phi)$ can be expressed as

$$D(\phi) = D_0(1 + \alpha\phi),$$

where α is the virial coefficient of D and is related to interparticle forces. In Fig. 1(a) we show the plot between the experimentally calculated diffusion coefficients D and the volume fraction of the reverse micelles, ϕ . A linear fit is seen to connect the points. This shows that the radius of the reverse micelles is nearly constant for a certain volume fraction ϕ , for the range of ϕ employed in this work.

Another value that characterizes reverse micelles is an estimate of the water-surfactant molar ratio W_0 in the limit of vanishing diffusion. This estimate is obtained from the plot of D as a function of W_0 . The plot is shown in Fig. 1(b), which can be fitted to a straight line. This allows an estimation of W_0 when $D \rightarrow 0$. By doing this we obtain a value of $W_0=21.6$ for ZnS and a value of $W_0=17.3$ for $\text{Zn}_{1-x}\text{Mn}_x\text{S}$. Experimentally, we have obtained visibly clear solutions of reverse micelles until $W_0=20$, above which turbidity results. This observation is approximately consistent with the upper limit of W_0 obtained from the plots in Fig. 1(b). Hence for the two systems the maximum sizes of the reverse micelles were limited to correspond to $W_0=12$.

In Fig. 2 we show the UV-visible spectra, obtained in solution, of reverse micelles under various conditions. The lowest line is for pure reverse micelles, empty, while those above this are for reverse micelles containing the reactants Na_2S and $\text{Zn}(\text{NO}_3)_2$, and the topmost plot is from the reaction product ZnS. The strong absorption peak at 223 nm is clearly from the AOT molecules and is common to all the systems. The characteristic absorption peaks due to the ZnS nanoparticles appear in the range 250–330 nm and this peak position reflects the band gap of the particles. These results are similar to recent reports in the literature⁷ for optical absorption in nanometer-sized reverse micelles. The absorption

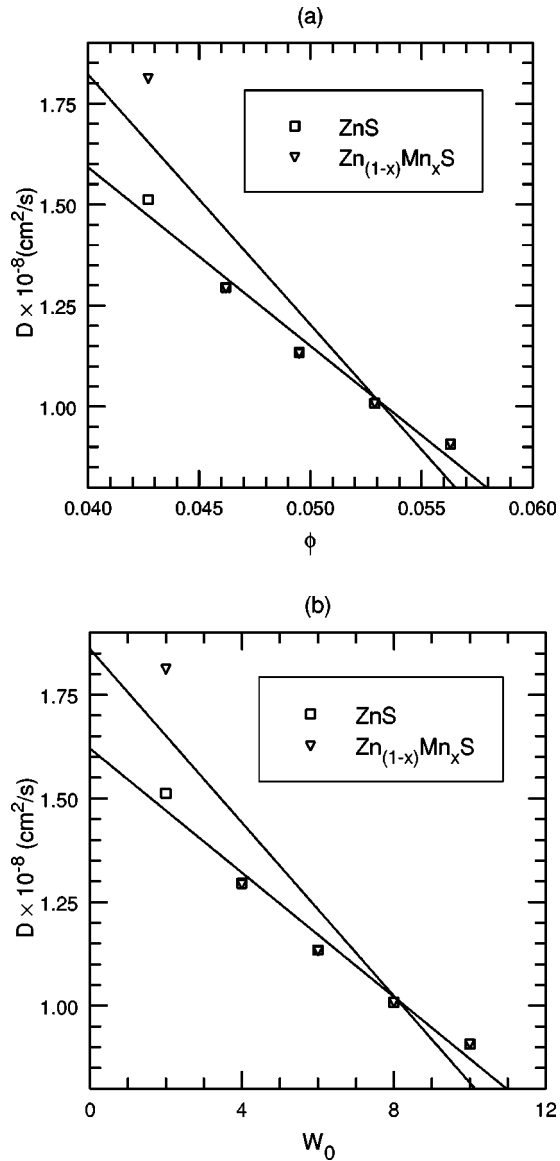


FIG. 1. The diffusion coefficients measured employing dynamic light scattering of reverse micelles containing ZnS and $\text{Zn}_{(1-x)}\text{Mn}_x\text{S}$, (a) as a function of the volume fraction of reverse micelles, ϕ , and (b) as a function of the water-surfactant molar ratio W_0 .

due to AOT is shifted for ZnS, possibly due to complex formation, but it is not important for this study.

In Figs. 3(a) and 3(b) we show the UV-visible spectra of ZnS and $\text{Zn}_{(1-x)}\text{Mn}_x\text{S}$ ($x=0.01$) in the reverse micellar form, after reaction. For both systems the data presented are for $W_0=2, 4, 6, 8, 10$, and 12. The AOT-derived strong peak is present at 250 nm for all the plots, while the peaks reflecting absorption by ZnS accompany this peak at higher wavelengths, $\lambda \geq 250$. In order to see the W_0 dependence of peak position and shape, we show in the inset to the plots an enlargement of this region. It is clear from the inset to Fig. 3(a) that the rising part of the peak, above background (the absorption edge), varies with W_0 . A careful study also shows a shift in peak position to higher λ with W_0 (redshift). A similar situation is observed in Fig. 3(b) for $\text{Zn}_{(1-x)}\text{Mn}_x\text{S}$.

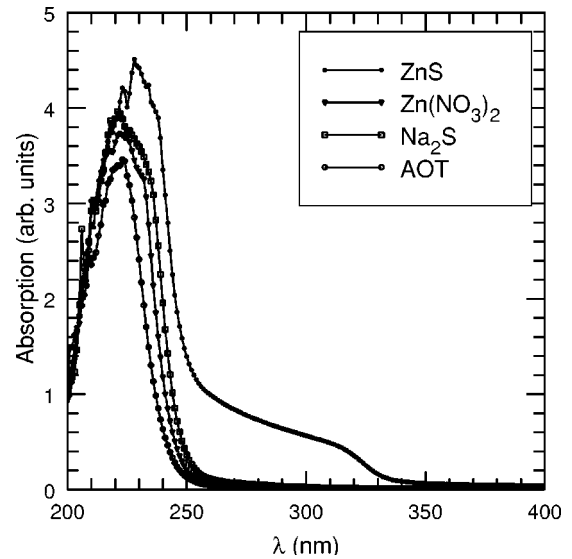


FIG. 2. UV-visible absorption spectra of reverse micelles containing AOT (open circles), Na_2S (open squares), $\text{Zn}(\text{NO}_3)_2$ (open squares), and ZnS (inverted triangles) at $W_0=10$ are compared.

There is, however, an important difference in the dependence on W_0 for the two systems. While in ZnS the variation in peak position is substantial, the variation in $\text{Zn}_{(1-x)}\text{Mn}_x\text{S}$ is reduced. Also, in the former, the absorption edge presents a systematic shift while in the latter this shift is negligible; moreover, the edge is present at a lower λ (higher energy) for the latter.

In order to quantify this we perform an exercise to identify the peak positions in the best possible way. The plots shown in the insets to Figs. 3(a) and 3(b) are first differentiated. The wavelengths corresponding to the maxima in the differentiated plots are then recorded, converted into energy, and plotted as a function of W_0 . This does not give the precise value of the peak position and hence the band gap E_g of zinc sulfide but is related by a linear constant.

In Fig. 4 we plot the band gaps obtained this way as a function of W_0 for ZnS and $\text{Zn}_{(1-x)}\text{Mn}_x\text{S}$. The following observations are readily made. The Mn doping of ZnS produces particles that are in general smaller than in the parent compound for the entire range of W_0 investigated. The data for $\text{Zn}_{(1-x)}\text{Mn}_x\text{S}$ also show an interesting trend. After a certain W_0 , the band gap does not change, reaching a minimum of approximately 3.88 eV. These band gap estimates are larger (blueshifted) than the bulk band gap of ZnS $E_g^b = 3.54$ eV,⁸ due to nanometer-sized particles. The points in Fig. 4 can be fitted to an expression relating the band gap E_g with W_0 given by $E_g = ae^{-W_0/b} + ce^{-W_0/d}$, where a, b, c, d are constants. This fit is shown in Fig. 4 as a continuous line connecting all the points. It is clear that the ZnS particle sizes continuously scale with the size of the reverse micelles the particles were created in. When extended to $W_0=20$, the reverse micellar method of study fails, but the particles can be extracted and the band gap measured from the resultant powder. On doing this a value of 3.73 eV is obtained, which is close to the extrapolated result for ZnS particles from Fig. 4.

The particle sizes can be estimated from a procedure

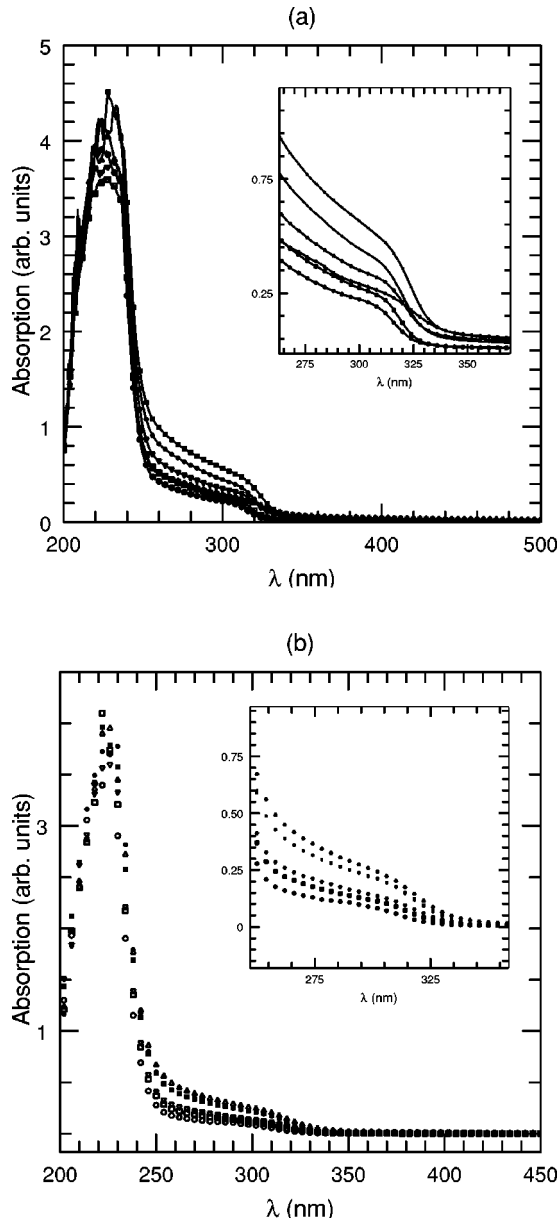


FIG. 3. (a) UV-visible absorption spectra are shown for ZnS containing reverse micelles for $W_0=2$ (open circles), 4 (open squares), 6 (inverted triangles), 8 (closed circles), 10 (closed squares), and 12 (triangles). The inset shows an expanded view of the region $\lambda=265\text{--}365$ nm. (b) UV-visible absorption spectra are shown for $\text{Zn}_{(1-x)}\text{Mn}_x\text{S}$ containing reverse micelles for $W_0=2$ (open circles), 4 (open squares), 6 (inverted triangles), 8 (closed circles), 10 (closed squares), and 12 (triangles). The inset shows an expanded view of the region $\lambda=265\text{--}340$ nm.

given in the literature by Rosetti *et al.*⁹ For Mn-doped ZnS, above $W_0=6$ (maximum reverse micellar size 3 nm, Table I), the largest particle size corresponding to 3.88 eV would be 60 Å. As our method outlined above underestimates the gap, this is in reasonable agreement; the actual gap is much larger and consequently smaller particles are present. The restriction in particle size due to Mn doping is interesting. Considering the nanoparticles as low-dimensional systems, we can extend arguments based on low-dimensional film growth theory. It is easily seen that the method in which film

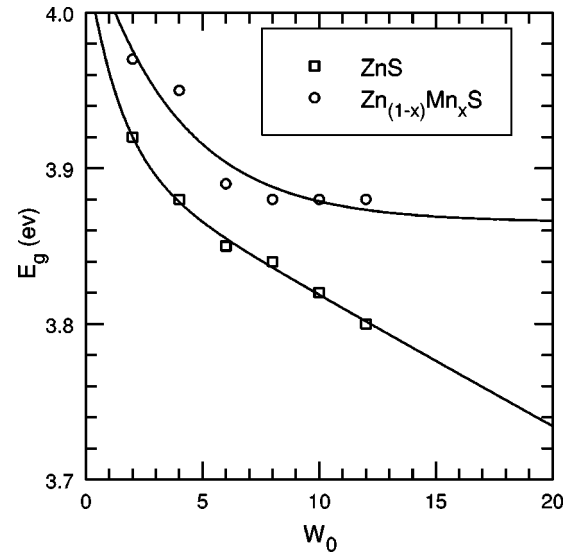


FIG. 4. The measured band gaps of ZnS and $\text{Zn}_{(1-x)}\text{Mn}_x\text{S}$ in the reverse micellar form (see text) are plotted as a function of W_0 . The fitted line has the functional form $E_g = ae^{-W_0/b} + ce^{-W_0/d}$ where a, b, c, d are constants.

growth takes place follows minimum free energy principles. Thus, during growth, for placement of an additional atom the change in free energy $\delta\sigma = \delta\sigma_o + \delta\sigma_i + \delta\sigma_s$, where σ_o , σ_i , and σ_s are the specific surface free energies for the overlayer, overlayer-substrate interface and the substrate, respectively. If $\delta\sigma$ is negative when a surface atom is added then growth takes place layer by layer. This is what occurs in ZnS. But on Mn doping, it is expected that the overlayer will take on the lattice parameter and the crystal symmetry of MnS during growth. Bulk MnS exists in halite (NaCl), wurtzite (hexagonal), and sphalerite (cubic) structures. While ZnS can exist in the halite as well as the wurtzite (or zinc blende) form, the latter is more abundant.¹⁰ This lattice mismatch can introduce a strain during the growth of ZnS in the presence of Mn, resulting in the accumulation of large strain energies. Strain energies are released by a breakdown in growth through the formation of dislocations, for example, which can result in crack formation. This naturally curtails the growth of ZnS particles in the presence of Mn impurities.

We also investigated the possibility of incorporating other magnetic impurities such as Fe and Ni. The interest here arises from the structural relationship of the sulfides of these transition metals with the host material ZnS. While ZnS and MnS are grossly isostructural, this is not so for the sulfides of Fe and Ni. These crystallize in the NiAs structure, where each S atom is surrounded by a trigonal prism of six metal (M) atoms ($M = \text{Fe}$ and Ni) and each metal atom has eight-fold coordination, comprising six S atoms and two other metal atoms. This is contrasted with the wurtzite structure of ZnS and MnS, where the metal as well as the S atoms are tetrahedrally bonded. This additional discrepancy of the desired symmetry between the host and dopant lattices would put severe restriction on their incorporation. This could lead to a total rejection of the dopant, in which case substitution will not modify the particle size. But if incorporated the desired strain could be achieved with less effort (reduced substitution).

TABLE II. The measured band gaps of $\text{Zn}_{(1-x)}\text{Mn}_x\text{S}$, $\text{Zn}_{(1-x)}\text{Fe}_x\text{S}$, and $\text{Zn}_{(1-x)}\text{Ni}_x\text{S}$ nanoparticles at various concentrations ($x=0.01, 0.02,$ and 0.03).

W_0	x			Compound
	0.01	0.02	0.03	
2	3.97	3.86	4.04	$\text{Zn}_{(1-x)}\text{Mn}_x\text{S}$
4	3.95	3.86	3.99	
6	3.89	3.85	3.92	
8	3.88	3.83	3.89	
10	3.88	3.84	3.86	
12	3.88	3.83	3.86	
2	3.89	4.27	4.10	$\text{Zn}_{(1-x)}\text{Fe}_x\text{S}$
4	3.83	4.21	4.07	
6	3.81	4.18	3.86	
8	3.81	4.13	3.86	
10	3.84	4.18	3.83	
12	3.82	4.18	3.84	
2	3.85	4.27	4.00	$\text{Zn}_{(1-x)}\text{Ni}_x\text{S}$
4	3.82	4.15	3.94	
6	3.82	4.13	3.94	
8	3.85	4.15	3.87	
10	3.82	4.13	3.84	
12	3.81	4.15	3.83	

The estimated band gaps of ZnS following substitution with Mn, Fe, and Ni are compared in Table II for three dopant concentrations with $x=0.01, 0.02,$ and 0.03 for each dopant. The results are encouraging and show that Fe and Ni substitutions are incorporated in the host ZnS lattice as seen by variation in the band gap (and hence the particle size) of the composite. For the lowest volume fraction W_0 (vessel size) the band gaps are largest for Fe and Ni substitutions. But the ultimate band gap achieved has a sharp dopant concentration dependence and seems to peak for a concentration of $x=0.02$ in this study, falling off at larger values of x , while for Mn doping the peaking has not been achieved for the range of x values studied. This could mean a gradual acceptance of Mn as a dopant by the host ZnS lattice as their structures are similar.

A relationship with the reported optical properties of the ZnS nanoparticles is suggested. From our results, it is clear that doping controls the smallest achievable particle sizes. The modified optical properties (enhanced photoluminescence) of ZnS can now be related to the theoretical investigation of the oscillator strength of a transition that finally produces the quantum efficiency for photoluminescence. The oscillator strength f_{ks} for transition from a state s to a state k was studied theoretically by Kayanuma.¹¹ In the region of strong confinement, the oscillator strength per unit volume was shown to increase dramatically in the region $2 \leq R/a_B \leq 4$ (R is the radius of the particle and a_B is the Bohr radius). From the definition of oscillator strength, this is due to the large overlap between the electron and hole wave functions in the confinement of the atomlike entities. Experimental observation of atomlike densities of states have indeed been reported for semiconductor nanostructures.^{12,13}

In view of this result it was tempting to produce $\text{Zn}_{(1-x)}\text{Mn}_x\text{S}$ in a large beaker (50 ml capacity) and look at the particle size without taking the reverse micellar route. The results are encouraging and particle sizes comparable to those reported here are obtained. For the Mn-doped samples, we observe photoluminescence peaks due to Mn at 580 nm and also higher photoluminescence in accordance with previous reports,¹ and a detailed study with variation in the Mn content x is in progress. But the importance of a local probe, such as scanning probe microscopy, for investigation of local electronic properties cannot be overestimated. This is in progress as well.

In conclusion, we have provided a systematic study of the role played by substituted magnetic impurities in determining the ultimate particle size that can be achieved in preparing semiconductor nanoparticles of ZnS. We have shown that the size of the particles is restricted on substitution, resulting in the natural formation of relatively smaller nanoparticles. The role played by the structure of the ZnS host material in relation to the substituted metal sulfides that occupy the host lattice in small quantities has been demonstrated.

We thank the Inter-University Consortium, Nuclear Science Center, New Delhi, for help with the UV-visible measurements.

*Author to whom correspondence and requests for materials should be addressed. Email address: psen@jnuv.ernet.in

¹R.N. Bhargava, D. Gallagher, X. Hong, and N. Nurmikko, Phys. Rev. Lett. **72**, 116 (1994).

²T.A. Kennedy, E.R. Glaser, P.B. Klein, and R.N. Bhargava, Phys. Rev. B **52**, R14 356 (1995).

³M.P. Pileni, J. Phys. Chem. **97**, 6961 (1993).

⁴B.J. Berne and R. Pecora, *Dynamic Light Scattering* (Wiley-Interscience, New York, 1976).

⁵A.M. Cazabat and D. Langevin, J. Chem. Phys. **74**, 3148 (1981).

⁶ ϕ is defined as $(V_{\text{AOT}} + V_{\text{H}_2\text{O}} + V_{\text{Reagent}})/(V_{\text{AOT}} + V_{\text{H}_2\text{O}} + V_{\text{Reagent}} + V_{\text{oil}})$.

⁷H. Sato, T. Ohtsu, and I. Komasa, J. Chem. Eng. Jpn. **32**, 300 (1999).

⁸Y. Zhang, N. Raman, J.K. Bailey, C.J. Brinker, and R.M. Crooks, J. Phys. Chem. **96**, 9098 (1992).

⁹R. Rossetti, R. Hull, J.M. Gibson, and L.E. Brus, J. Chem. Phys. **82**, 552 (1985).

¹⁰L.V. Azaroff, *Introduction to Solids* (Tata McGraw-Hill, New Delhi, 1990), p. 366.

¹¹Y. Kayanuma, Phys. Rev. B **38**, 9797 (1988).

¹²M. Grundmann *et al.*, Phys. Rev. Lett. **74**, 4043 (1995).

¹³U. Banin, Y. W. Cao, D. Katz, and O. Millo, Nature (London) **400**, 542 (1999).